Magnetic structure of Sm₂IrIn₈ determined by x-ray resonant magnetic scattering

C. Adriano,[1,*] R. Lora-Serrano,[1] C. Giles,[1] F. de Bergevin,[2] J. C. Lang,[3] G. Srajer,[3] C. Mazzoli,[2]
L. Paolasini,[2] and P. G. Pagliuso[1]

[1]*Instituto de Física "Gleb Wataghin," UNICAMP, 13083-970 Campinas-SP, Brazil*
[2]*European Synchrotron Radiation Facility, Grenoble 38043, France*
[3]*Advanced Photon Source, Argonne National Laboratory, Argonne, Illinois 60439, USA*
(Received 22 April 2007; published 21 September 2007)

The magnetic structure of the intermetallic antiferromagnet Sm₂IrIn₈ was determined using x-ray resonant magnetic scattering. Below $T_N = 14.2$ K, Sm₂IrIn₈ has a commensurate antiferromagnetic structure with a propagation vector $\vec{\eta} = (1/2, 0, 0)$. The Sm magnetic moments lie in the *ab* plane and are rotated roughly 18° away from the *a* axis. The magnetic structure of this compound was obtained by measuring the strong dipolar resonant peak whose enhancement was of over 2 orders of magnitude at the L_2 edge. At the L_3 edge, both quadrupolar and dipolar features were observed in the energy line shape. The magnetic structure and properties of Sm₂IrIn₈ are found to be consistent with the general trend already seen for the Nd-, Tb-, and the Ce-based compounds from the $R_m M_n \text{In}_{3m+2n}$ family (R = rare earth; M = Rh or Ir; m = 1, 2; n = 0, 1), where the crystalline electrical field effects determine the direction of magnetic moments and the T_N evolution in the series. The measured Néel temperature for Sm₂IrIn₈ is slightly suppressed when compared to the T_N of the parent cubic compound SmIn₃.

PACS number(s): 71.20.Lp, 75.25.+z, 75.50.Ee, 75.30.−m

I. INTRODUCTION

The microscopic details of 4*f*-electron magnetism play a fundamental role in the physical properties of various classes of rare-earth-based materials such as heavy fermions, magnetically ordered alloys, and permanent magnets. The existence of structurally related families of rare-earth-based compounds provides a great opportunity to explore how the details of the 4*f*-electron magnetism evolve as a function of changes in the dimensionality, local symmetry, and electronic structure along each related family. The recently discovered[1–8] family of intermetallic compounds $R_m M_n \text{In}_{3m+2n}$ (M = Co, Rh or Ir, m = 1, 2; R = La, Ce, Pr, Nd, Sm, Gd) have proved to be very promising in this regard since it possesses many members of structurally related heavy-fermion superconductors (HFS), for R = Ce, antiferromagnets (R = Nd, Sm, Gd, and Tb), and paramagnetic metals (R = La, Pr). Within this family, the physical properties of a particular R member can also be compared to compounds based on the same R with three different related structures [the cubic $R\text{In}_3$ and the tetragonal $R M \text{In}_5$(1-1-5) and $R_2 M \text{In}_8$ (2-1-8)][9–11] and/or to the same R formed with three distinct transition metals (M = Rh, Ir, and Co, not for all R) in the same structure.

For the Ce-based HFS in this family, extensive investigation has revealed fascinating physical properties such as quantum criticality, non-Fermi-liquid behavior, and an intriguing interplay between magnetism and superconductivity, reflected in very rich phase diagrams.[12–20] Because the HFS members of this family are structurally related, its investigation has been used to provide some insights on the question why some structure types are favorable to host many superconductors. A possible relationship between the superconducting critical temperature T_c and the crystalline anisotropy,[13,21,22] the role of the 4*f*-electron hybridization with the conduction electrons in the occurrence of superconductivity,[23–25] and the effects of quasi-two-dimensional electronic structures[26–28] are some of the physical phenomena

that have been brought to the scenario to answer the question above. Further, motivated by this experimental trend, new materials search based on the 1-1-5 structures has led to the discovery of the Pu-based HFS PuMGa₅ (M = Rh and Co).[29,30]

On the other hand, as these HFSs are presumably magnetically mediated, other studies[5–7,21,31–37] have been focused in understanding the evolution of the 4*f* local magnetism, not only for the magnetically ordered Ce-based members of this family such as CeRhIn₅ and Ce₂RhIn₈ but also for their antiferromagnetic counterparts $R_m M_n \text{In}_{3m+2n}$ (M = Rh or Ir, m = 1, 2) for R = Nd, Sm, Gd, and Tb. From these studies, the role of tetragonal crystalline electrical field (CEF) in determining the spatial direction of the ordered R moments with respect to the lattice and the evolution of the Néel temperature T_N in the series was established.[5–7,32,37]

A key set of experiments that has allowed the above conclusions was the experimental determination of the magnetic structures of various members of the $R_m M_n \text{In}_{3m+2n}$ (M = Rh or Ir, m = 1, 2) family.[7,31,36,38–41] To date, however, none of the Sm-based compounds from this family have had their magnetic structures determined. In fact, the compounds of this series containing Sm ions may be particularly important in testing the extension of the CEF trends in this family because the presence of excited J-multiplet states in Sm^{3+} and quadrupolar interactions have to be taken into account in order to understand their magnetic phase diagrams.[42–45] Especially interesting is Sm₂IrIn₈ which presents a first order antiferromagnetic transition at $T_N = 14.2$ K.[5] This value is slightly smaller than the $T_N \sim 16$ K of the cubic SmIn₃,[11] which according to the CEF trends observed in other members of this family[7,37] suggest that the ordered Sm moments should lie in the *ab* plane.

To further explore the magnetic properties of Sm₂IrIn₈ and to check the extension of the CEF trends observed for R = Nd, Tb, and Ce,[5–7,32,37] to the Sm-based compounds, we report in this work the solution of the magnetic structure of the intermetallic antiferromagnet Sm₂IrIn₈ by means of the

x-ray resonant magnetic scattering (XRMS) technique. The XRMS technique has proved to be a very important tool for the investigation of microscopic magnetism in condensed matter, especially for highly neutron absorber ions such as Sm, where the often preferred technique of neutron scattering becomes nearly prohibitive.

Sm_2IrIn_8 presents, below $T_N = 14.2$ K, a commensurate antiferromagnetic structure with a propagation vector $\vec{\eta} = (\frac{1}{2}, 0, 0)$ and Sm magnetic moments lying in the *ab* plane. In terms of relative orientation, the propagation vector $\vec{\eta}$ indicates that the Sm spins are ordered antiferromagnetically along the *a* axis and ferromagnetically along the *b* axis and, because of the presence of two Sm ions per unit cell along the *c* axis, some calculations have to be performed in order to determine the type of ordering along this direction. Furthermore, as it could be expected for such spin arrangement in a tetragonal compound, antiferromagnetic domains were observed in the ordered state of Sm_2IrIn_8. These domains were removed by field cooling the sample at a field of $H = 10$ T.

II. EXPERIMENT

Single crystalline samples of Sm_2IrIn_8 were grown from indium flux as described previously.[5,46] The crystal structure, unit cell dimensions, and macroscopic properties of the Sm_2IrIn_8 single crystals used in this work were in agreement with the data in Ref. [5]. For the XRMS experiments of this work, selected crystals were extracted and prepared with polished $(0, 0, l)$ flat surfaces and sizes of approximately $4 \times 3.4 \times 1.5$ mm^3. The preferred crystal growth direction of this tetragonal compound is columnar along the $[00l]$ direction and the (001) facet is relatively large. The mosaic spread of the sample was found to be $< 0.08°$ by a rocking curve (θ scan) on a Phillips four circle diffractometer.

XRMS studies were performed at the 4-ID-D beamline at the Advanced Photon Source (APS) and at the ID-20 beamline at the European Synchrotron Radiation Facility (ESRF). The 4-ID-D x-ray source is a 33 mm period planar undulator and the energy is selected with a double crystal Si(111) monochromator. A toroidal mirror focuses the beam to a 220 μm (horizontal) $\times$ 110 μm (vertical) spot, yielding an incident flux of $\sim 3.5 \times 10^{13}$ photons/s with an energy resolution of $\delta E/E = 1.4 \times 10^{-4}$. The sample was cooled in a closed-cycle He refrigerator (with a base temperature of 4 K) with a dome Be window. Our experiments were performed in the coplanar geometry with σ-polarized incident photons, i.e., in the vertical scattering plane, using a four-circle diffractometer. Except for azimuthal scans, the sample was mounted with the *b* axis perpendicular to the scattering plane.

In most measurements, we have performed a polarization analysis, with Cu(220), Graphite (006), and Au(111) crystal analyzers, appropriate for the energies of Sm L_2 and L_3 edges. The diffractometer configuration at the APS allowed measurements at different azimuthal angles (ϕ) by rotating the sample around the scattering vector **Q**. This was particularly useful to probe the magnetic moment components at the dipolar resonant condition with σ incident polarization.
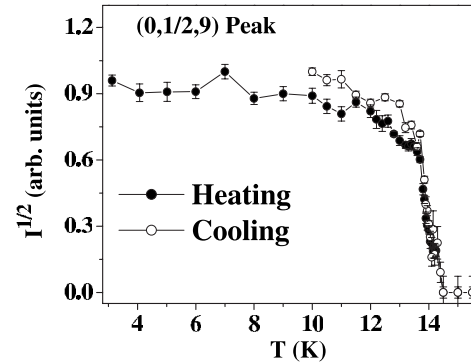

FIG. 1. Temperature dependence of the magnetization of Sm_2IrIn_8 measured with transverse (θ) scans at the $(0, \frac{1}{2}, 9)$ peak.

The x-ray source on the ID-20 beamline was a linear undulator with a 32 mm period. The main optical components are a double Si(111) crystal monochromator with sagital focusing and two meridional focusing mirrors on either side of the monochromator. At 7.13 keV using the first harmonic of the undulator u32, the standard incident flux at the sample position was approximately 1×10^{13} photons/s at 200 mA with a beam size of 500 μm (horizontal) $\times$ 400 μm (vertical). The sample was mounted on a cryomagnet (with a base temperature of 2 K), installed on a horizontal six-circle diffractometer, with the *b* axis parallel to the cryomagnet axis and perpendicular to the scattering plane. This configuration allowed π-polarized incident photons in the sample and the application of an external magnetic field up to 10 T perpendicular to the scattering plane.[47]

III. RESULTS

A. Temperature dependence and resonance analysis

Magnetic peaks were observed in the dipolar resonant condition at temperatures below $T_N = 14.2$ K at reciprocal lattice points forbidden for charge scattering and consistent with an antiferromagnetic structure with propagation vector $(\frac{1}{2}, 0, 0)$. Their temperature dependence was studied for increasing and decreasing temperature sweeps. Figure 1 shows the temperature dependence of $(0, \frac{1}{2}, 9)$ magnetic reflection at an incident photon energy of 7.313 keV (L_2 edge) and measured at π incident polarization without polarization analysis. The squared root of the integrated intensity which is proportional to the magnetic moment component of the Sm atom is displayed in Fig. 1. A pseudo-Voigt peak shape was used to fit transversal θ scans through the reciprocal lattice points in order to obtain the integrated intensities of the reflection peak. This peak intensity decreases abruptly to zero for $T > 13$ K and its critical behavior cannot be described by a power-law function with a critical exponent β. This result is in agreement with the first order character of the magnetic transition at 14.2 K, revealed by heat capacity data, from which a latent heat of ~ 10 J/mol was extracted.[5] Consistently, we found evidence of small hysteresis for $T \lesssim 14.2$ when changing from warming to the cooling temperature sweep.
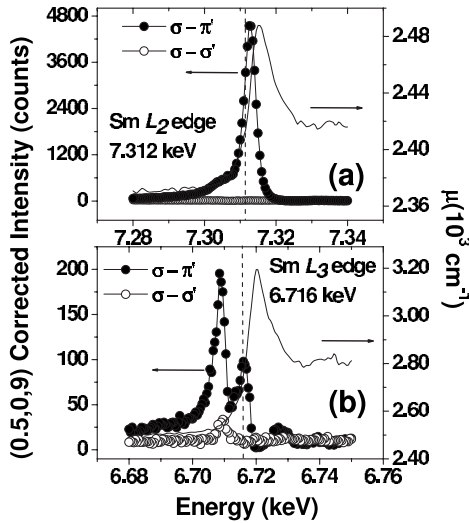
FIG. 2. Energy scan of the $\left(\frac{1}{2},0,9\right)$ magnetic peak at $T=5.9$ K for σ-π' (closed circles) and σ-σ' (open circles) polarization channels at the L_2 (top) and L_3 (bottom) absorption edges. The data have been corrected for absorption, $\mu(E)$, using the measured fluorescence yield. Arrows indicate the scales for the fluorescence yield (right) and the observed data (left). The vertical dashed lines show the energy positions of the absorption edges for Sm L_2 edge ($E=7.312$ keV) and Sm L_3 edge ($E=6.716$ keV).

The energy line shape curves for the polarization channels σ-π' and σ-σ' of the $\left(\frac{1}{2},0,9\right)$ diffraction peak at (a) the L_2 and (b) the L_3 absorption edges of Sm^{3+} ion at $T=5.9$ K are shown in Fig. 2. The solid lines in both panels represent the absorption spectrum, $\mu(E)$, extracted from fluorescence yield. The data of Fig. 2 were collected at the 4-ID-D beamline of APS by counting the photons reaching the detector at a fixed **Q** while changing the incident energy. The strong resonant enhancement of the x-ray scattering at this reciprocal space position provides clear evidence of the magnetic origin of the observed peaks.

The energy line shape curve in Fig. 2(a) has a maximum at 7.312 keV, which is only ~2.5 eV larger than the L_2 absorption edge (defined by the inflection point of the absorption spectrum), revealing the electric dipolar character ($E1$) of this transition (from $2p$ to $5d$ states). Figure 2 also shows the polarization analysis that was performed in order to unambiguously confirm the magnetic origin of the superstructure peaks. Polarization analysis was also used to verify whether the anomaly at approximately 8 eV below the dipolar peak in Fig. 2(a) could be associated with a quadrupolar transition[48] or it simply represents an enhanced interference between the nonresonant and the resonant part of the scattering amplitude. For the experimental configuration used (incident σ polarization), the electric dipole transitions $E1$ rotate the plane of polarization into the scattering plane (π polarization). Our data in Fig. 2(a) reveal a strong enhancement of the scattered intensities at the σ-π' channel (closed circles) and no enhancement at the σ-σ' channel for the same energy range. These results confirm the magnetic origin of the $(h,0,l)\pm\left(\frac{1}{2},0,0\right)$ reflections due to the existence of an

antiferromagnetic structure doubled along the crystallographic $\hat{a}$ direction, with a propagation vector $\vec{\eta}=\left(\frac{1}{2},0,0\right)$.

The energy line shape around the Sm L_3 edge is presented in Fig. 2(b). Firstly, the observed intensities are roughly 1 order of magnitude weaker than those obtained at the L_2 resonance consistent with previous measurements on pure Sm.[45] Secondly, there are two peaks in the σ-π' channel signal, as also observed for other light rare-earth[49,50] and Sm-based compounds.[45,51] A high energy peak appears at 6.716 keV, while a low energy and more intense enhancement can be observed at 6.708 keV. Interestingly, Stunault *et al.*[45] have demonstrated that for pure Sm, the quadrupolar $E2$ resonance is more intense than the dipolar $E1$ at the L_3 edge and they found that the energy difference between the $E2$ and the $E1$ resonance is of the order of 8 eV, the same as the one found in this work. Furthermore, in the σ-σ' channel, only an enhancement at 6.708 keV could be observed, which is consistent with the quadrupolar character of this resonance, since the scattering signal in σ-σ' channel for dipolar transitions is strictly forbidden (see Refs. 48 and 52). Thus, the presence of this preedge enhancement in the energy curves of Fig. 2 confirms an expected quadrupole ($E2$) $2p$ to $4f$ contribution to the resonant x-ray scattering in Sm$_2$IrIn$_8$.

B. Magnetic structure

The magnetic structure of the Sm$_2$IrIn$_8$ was experimentally investigated using dipolar resonant x-ray magnetic scattering with polarization analysis. In general, the magnetic scattering intensities are given by[48,51]

$$I \propto \frac{1}{\mu^* \sin(2\theta)}\left|\sum_n f_n^{XRES}(\vec{k},\hat{\epsilon},\vec{k}',\hat{\epsilon}')e^{i\vec{Q}\cdot\vec{R}_n}\right|^2, \quad (1)$$

where μ^* is the absorption correction for asymmetric reflections, 2θ is the scattering angle, $\vec{Q}=\vec{k}'-\vec{k}$ is the wave-vector transfer, $\vec{k}$ and $\vec{k}'$ ($\hat{\epsilon}$ and $\hat{\epsilon}'$) are the incident and scattered wave (polarization) vectors, respectively. $\vec{R}_n$ is the position of the nth atom in the lattice and $\hat{z}_n$ is the moment direction at the nth site. The resonant scattering amplitude contains both dipole ($E1$) and quadrupole ($E2$) contributions. For the determination of the magnetic structure of this work, we have used the second term of the electric dipole transition ($E1$) form factor which produces magnetic peaks. In this case, we have

$$f_{nE1}^{XRES} \propto \begin{bmatrix} 0 & \hat{k}\cdot\hat{z}_n \\ -\hat{k}'\cdot\hat{z}_n & (\hat{k}'\times\hat{k})\cdot\hat{z}_n \end{bmatrix}$$
$$\propto \begin{bmatrix} 0 & z_1\cos\theta+z_3\sin\theta \\ -z_1\cos\theta+z_3\sin\theta & -z_2\sin(2\theta) \end{bmatrix}, \quad (2)$$

where θ is the Bragg angle, z_1, z_2, and z_3 are the components of the magnetic moment at the nth site, according to the commonly used geometry convention of Ref. 53, and σ, π, σ' and π' describe the incident (nonprimed terms) and scattered (primed) photon polarizations.

TABLE I. Comparison between observed and calculated intensities of magnetic Bragg reflections, assuming either parallel (model I) or antiparallel (model II) alignment between the moments of two Sm ions along the c axis in the same chemical unit cell.

(h,k,l)	Expt. data	Model I		Model II	
		$\mathbf{m}\|c$	$\mathbf{m}\|a$	$\mathbf{m}\|c$	$\mathbf{m}\|a$
$(1/2,0,6)$	66	13	29	24	55
$(1/2,0,7)$	78	17	29	39	68
$(1/2,0,8)$	5	77	100	3.4	4.5
$(1/2,0,9)$	100	3	3	100	100
$(1/2,0,10)$	12	100	68	32	23

As described previously, two experimental setups have been used in this work, in the vertical (4-ID-D beamline) and horizontal (ID-20) scattering configurations. This permitted us to access all four polarization channels of the 2×2 matrix in Eq. (2) and to determine the magnetic moment orientations through their polarization dependence at the $E1$ resonance by comparing the relative intensities of experimental $\left(\frac{1}{2},0,l\right)$ magnetic peaks with the calculated ones using the appropriate terms of matrix (2).[51]

In the case of Sm_2IrIn_8, the magnetic propagation vector $\vec{\eta}=\left(\frac{1}{2},0,0\right)$ does not unequivocally determine the magnetic structure due to the presence of two magnetic Sm atoms per chemical unit cell along the $\hat{c}$ direction. Therefore, as stated above, we have an antiparallel ordering of the Sm moments along the $\hat{a}$ direction and a parallel ordering along $\hat{b}$. Along $\hat{c}$, there are, however, two possibilities of coupling that can take place: a parallel arrangement (model I), in which the moments of neighboring Sm ions along the c axis are parallel to each other (sequence $++$ $++$ $++\cdots$), or the antiparallel coupling (model II), with the sequence $+-$ $+-$ $+-\cdots$. These two possibilities have been considered in the calculated magnetic structure factor while orienting the magnetic moment along the three crystallographic directions for five different $\left(\frac{1}{2},0,l\right)$ magnetic Bragg peaks, with $l=6,7,8,9,10$. The calculated intensities are strongly dependent on the projections of magnetic moments along the crystallographic axis through the $f^{\sigma\pi'}$ term of Eq. (2). The calculated intensities were compared to the relative intensities of the experimental results for each case. This evaluation was performed at the vertical geometry of the 4-ID-D beamline at 9 K, by performing rocking scans with the crystal analyzer and numerically integrating the data.[51] We show this analysis in Table I, where "model I" stands for the $++$ $++$ $++\cdots$ sequence and "model II" for the $+-$ $+-$ $+-\cdots$ one. This comparison shows that the model which best fits the experimental data is the one assuming antiparallel coupling along the c axis (model II) with the magnetic moments approximately oriented along the a axis [according to matrix (2), for a σ-polarized incident beam and peaks at reciprocal space positions with the (001) normal surface contained in the scattering plane, contributions from an oriented moment along $\hat{b}$ direction cannot be detected].
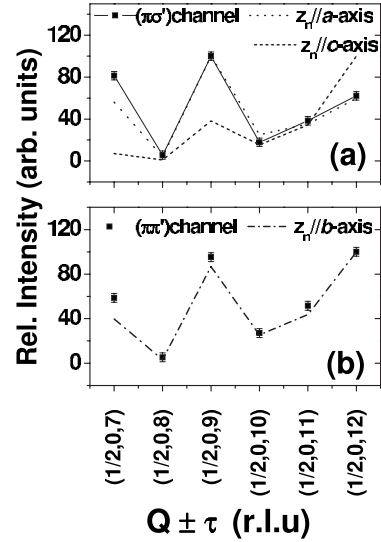

FIG. 3. Analysis of the possible magnetic moment directions for Sm_2IrIn_8 at the L_2 resonance. $\mathbf{Q}$ dependence of the integrated intensities of (a) six satellite peaks signal in the π-σ' channel with the moments along $\hat{a}$ and $\hat{c}$ and (b) in the π-π' with moments parallel to $\hat{b}$.

In addition, we have also measured the π-σ' and π-π' polarization channels at the horizontal geometry of the ID-20 beamline. Measuring these two channels, we gained access to the z_1 and z_3 components [in Eq. (2)] of magnetic moment vector in one case [π-σ', Fig. 3(a)] and to z_2 in the other [π-π', Fig. 3(b)]. There is a clear indication that for the π-σ' channel, the observed data are well fit when considering the moments along the $\hat{a}$ direction [dotted curve in Fig. 3(a)] instead of the $\hat{c}$ direction (short dashed curve). Also in this case, the $E1$ terms are not sensitive to the component of the ordered moment perpendicular to the scattering plane, i.e., along the b axis. Further, when measuring the channel $(\pi$-$\pi')$, we are only allowed to measure the b component, which is confirmed by the good fit of experimental data when assuming magnetic moments along such direction [dash-dotted curve in Fig. 3(b)]. These two last results indicate that the Sm moments actually have components along both a and b real space axes and not perfectly aligned along any of these two directions.

To determine the exact orientation of the magnetic moments within the ab plane, we have performed azimuthal scans (ϕ scan) through the $\left(\frac{1}{2},0,9\right)$ reflection (Fig. 4) at the $E1$ resonance. At the σ-π' polarization channel, this procedure warrants the determination of moment directions with no ambiguity because the magnetic cross section is strongly dependent on the magnetic moment direction and the polarization of the incoming and scattered radiation; the maximum (minimum) intensity in the curve will occur with the magnetic moment being parallel (perpendicular) to the diffraction plane. With the experimental setup of 4-ID-D beamline, we had access to record points at azimuthal angles ϕ between $-50°$ and $60°$. In order to compare with the observed data, one can calculate the intensities for the σ-π' channel using expressions (1) and (2) and a reasonably
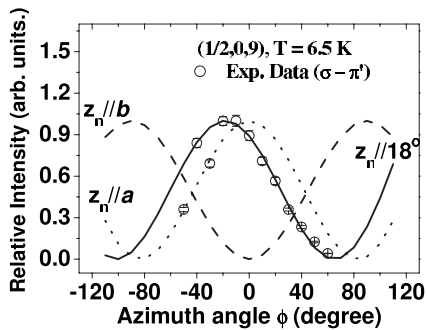
FIG. 4. Normalized relatively integrated intensities of the $\left(\frac{1}{2},0,9\right)$ magnetic peak at $T=6.5$ K (open circles) as a function of the azimuth angle. The other curves represent the variation expected for the magnetic moments along the $\hat{a}$ (dotted line), $\hat{b}$ (dashed line), and 18° away from $\hat{a}$ (solid line), directions.

simple geometry analysis considering the projections of both $\hat{k}'$ and $\hat{z_n}$ on the coordinate system of Ref. 53 when the azimuth angle is changed. Then, the calculated intensity is proportional to $I^{\sigma\pi'} \propto |-\cos\theta\cos\phi\cos\alpha + \sin\theta\sin\alpha|^2$, where α represents the asymmetry angle between the scattering and the normal surface vectors.[51] Figure 4 shows the experimental and the calculated relative intensities considering the moment along the a, b axis and 18° tilted from the a axis, which is the value that nicely adjust the experimental data. Considering the experimental errors we can then conclude that the magnetic moment is in the ab plane making $(18° \pm 3°)$ with the $\hat{a}$ direction of the sample. Using all the above results, a model of the magnetic unit cell of Sm$_2$IrIn$_8$ can be constructed and is shown in Fig. 5.

As it was observed in the magnetic structure of other members of the R_mMIn$_{3m+2}$ series such as NdRhIn$_5$,[38] TbRhIn$_5$,[7] GdRhIn$_5$,[41] and Gd$_2$IrIn$_8$,[36] the magnetic structure of Sm$_2$IrIn$_8$ presents a lower symmetry than the crystallographic structure, as the Sm spins present different relative orientations along the $\hat{a}$ and $\hat{b}$ directions even though a and b are indistinguishable. This spin arrangement was explained by considering the first (J_1) and second (J_2) R-neighbor exchange interactions in the case of a small J_1/J_2 ratio.[41]

Considering the observation of this kind of magnetic structure in tetragonal compounds, it may be expected that at
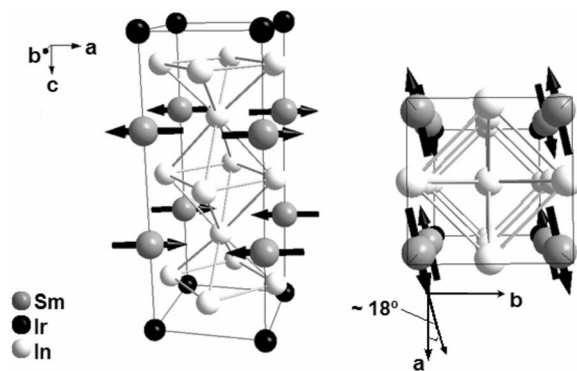

FIG. 5. Magnetic structure of Sm$_2$IrIn$_8$ below $T_N=14.2$ K (left) and a Sm-In plane top view (right) showing the arrangement of Sm moments within the SmIn$_3$ blocks.
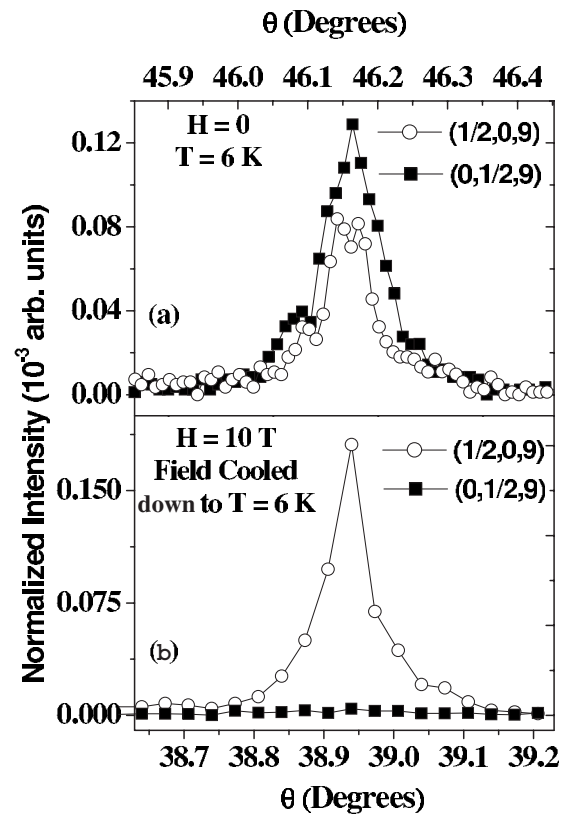

FIG. 6. Field dependence of the integrated intensities of the $\left(\frac{1}{2},0,9\right)$ and $\left(0,\frac{1}{2},9\right)$ magnetic peaks taken with transverse (θ) scans around each reciprocal space lattice points (top axis for open symbols and bottom axis for solid symbols). (a) For $H=0$ applied field at $T=6$ K and (b) field cooled from 16 to 6 K at $H=10$ T.

zero magnetic field, the antiferromagnetic ordering takes place with the formation of antiferromagnetic domains where the relative orientation of the magnetic moments along a given direction ($\hat{a}$ or $\hat{b}$) changes from parallel to antiparallel between the domains. The presence of a twinned magnetic structure with symmetry-related domains was evidenced by the observation of both $\left(\frac{1}{2},0,l\right)$ and $\left(0,\frac{1}{2},l\right)$ reflection types. To further investigate the presence of antiferromagnetic domains in the ordering state of Sm$_2$IrIn$_8$, we follow the behavior of the magnetic $\left(\frac{1}{2},0,l\right)$ and $\left(0,\frac{1}{2},l\right)$ reflections under an applied magnetic field.

Figure 6 presents the behavior of the $\left(\frac{1}{2},0,9\right)$ and $\left(0,\frac{1}{2},9\right)$ intensities as a function of the applied magnetic field of 10 T along one of the tetragonal axis in the plane (defined as the $\hat{b}$ direction). At zero field, both $\left(\frac{1}{2},0,9\right)$ (open circles) and $\left(0,\frac{1}{2},9\right)$ (closed squares) intensities can be observed at $T=6$ K with comparable magnitude [Fig. 6(a)] and the $\left(\frac{1}{2},0,9\right)$ intensity is roughly 66% that of the $\left(0,\frac{1}{2},9\right)$ peak. The sample was then field cooled ($H=10$ T) from the paramagnetic (16 K) to the ordered state (6 K) with the field applied along the $\hat{b}$ direction. As can be seen in Fig. 6(b), the $\left(0,\frac{1}{2},9\right)$ diffraction peak disappears as the magnetic field favors the parallel spin orientation along the b axis. The same effect was also observed for the other five $\left(0,\frac{1}{2},l\right)$ reflections (not shown). The results under applied magnetic field shown in

Fig. 6 confirm the existence of a twinned magnetic structure for Sm_2IrIn_8 which allows the observation of both $\left(0,\frac{1}{2},l\right)$ and $\left(\frac{1}{2},0,l\right)$ magnetic reflections at zero field.

IV. DISCUSSION

Early studies on the antiferromagnetic cubic compound $SmIn_3$ have shown multiple magnetic transitions associated with quadrupolar ordering and magnetoelastic and magnetocrystalline competitive effects at 14.7, 15.2, and 15.9 K (the former two temperatures being associated with successive magnetic dipolar and antiferromagnetic orders and the last one due to quadrupolar ordering).[42,43] For the tetragonal Sm_2IrIn_8, the insertion of any additional $SmIn_3$ atomic layers into the crystalline structure slightly decreases T_N compared to that of $SmIn_3$ (14.2 and 15.2 K for the Sm2-1-8 and Sm1-0-3 T_N's, respectively) and an additional anomaly at 11.5 K has been observed in the specific heat and resistivity measurements,[5] probably related to the successive transitions seen in the ordered phase of the $SmIn_3$.

Following the investigation of the isostructural magnetic non-Kondo compounds from the R_mMIn_{3m+2} family, where the details the $4f$ magnetism along the series may be important to understand the possible magnetic-mediated superconductivity in the compounds with R=Ce, we have studied the magnetic structure of Sm_2IrIn_8, which is the only compound from this family with a clear first order antiferromagnetic transition with a latent heat of ~ 10 J/mol,[5] and now it is the first Sm member of this family with a solved magnetic structure, which is the main result of this work. The determination of the Sm2-1-8 magnetic structure allows the investigation of the CEF driven trends of magnetic properties within the R_mMIn_{3m+2} family to be extended to the Sm-based members.

Our results confirm the complex resonance profile of Sm-based compounds (at one satellite reciprocal point, Fig. 2), as seen in previous studies of pure Sm.[45] It has been argued that the larger intensity of $E2$ resonance at Sm L_3 edge compared to its intensity at the L_2 edge may be explained qualitatively by the spin-orbit splitting of the intermediate $4f$ levels involved.[45] The L_3 transitions connect the $j=\frac{7}{2}$, state while L_2 involves transitions to the $j=\frac{5}{2}$ level, which lie lower in energy and therefore can be preferentially populated by the five $4f$ electrons of Sm^{3+}. This reduces the number of vacant $j=\frac{5}{2}$ states from 6 to 1, in contrast to the eight states available for the $j=\frac{7}{2}$, level, which increases the transition probability of the $E2$ resonance at Sm L_3 in Sm_2IrIn_8.

Considering the additional magnetic transitions observed for $SmIn_3$,[42,43] and the additional anomaly at $T=11.5$ K in heat capacity and electrical resistivity measurements for Sm_2IrIn_8,[37] we did not observe any discontinuities, within the resolution of our experiment, in the integrated intensities of the $\left(0,\frac{1}{2},9\right)$ magnetic peak from roughly 4 up to 16 K (Fig. 1). Therefore, we conclude that there are no changes of the magnetic propagation vector $\vec{\eta}=\left(\frac{1}{2},0,0\right)$ below T_N. For completeness, on going field-dependent heat capacity and thermal expansion measurements (not shown and will be published elsewhere) have revealed no field-induced transitions up to $H=9$ and 18 T, respectively, similar to $SmIn_3$

where no additional transition was found with applied field up to $H=32$ T.[44]

On the other hand, recent works have shown that the low temperature CEF configuration plays a fundamental role on the behavior of T_N and the magnetic moment directions within the R_mMIn_{3m+2} family.[7,32,37,40] Further, Kubo *et al.*[54] has also proposed an orbital controlled mechanism for superconductivity in the Ce-based compounds from this family. For the Sm members, CEF effects confine the magnetic moments to the ab plane, consistent with the experimental CEF trends observed for R=Ce, Nd, and Tb (Refs. 5–7 and 32) and also by the predictions of a recently developed mean-field theoretical model.[7,37] If the magnetic ordered moments lie in the ab plane but they are more magnetically susceptible along the c axis, the magnetic order can be frustrated to lower T_N values than for their cubic relatives. The mean-field model of Ref. 37, however, only includes the contributions of tetragonal CEF and first neighbor isotropic dipolar exchange interaction. Therefore, it may not be expected to work for Sm containing compounds because for the Sm^{3+} ion, the first excited J multiplet lying just above the ground state is closer in energy. Thus, the tetragonal CEF splitting can mix both the excited and ground state CEF schemes and therefore this mixture should be considered into the calculations. This effect is responsible for the nonlinear response of the inverse of magnetic susceptibility at high temperatures on $SmIn_3$ and other Sm-based compounds,[11,55] as well as in the measurements of Sm_2IrIn_8 of Ref. 5. Furthermore, as it was found for $SmIn_3$,[42,43] quadrupolar magnetic interactions also have to be considered in order to achieve a complete description of the magnetic properties of the Sm-based compounds in the R_mMIn_{3m+2} family.

Apart from the higher complexity of the magnetic properties of the Sm compounds, it was found experimentally that T_N is decreased (roughly $\sim 10\%$) for the tetragonal compounds when compared to the cubic $SmIn_3$. In addition, we have found that the magnetic structure of Sm_2IrIn_8 shows the ordered Sm moments in the ab plane, as expected in the case of T_N suppression.[7,37] Although the changes in T_N for the Sm compounds is much smaller (perhaps due to the particularities of the Sm^{3+} ion discussed above) than that observed for R=Ce, Nd, and Tb in the R_mMIn_{3m+2} family, we can conclude with the solution of the magnetic structure reported here that the general CEF trend of the R_mMIn_{3m+2} is also qualitatively present in Sm_2IrIn_8.

V. CONCLUSION

In summary, we have presented the results of the magnetic structure determination of the intermetallic antiferromagnet Sm_2IrIn_8. The magnetic order is commensurate with propagation vector $\vec{\eta}=\left(\frac{1}{2},0,0\right)$ and the Sm moments oriented in the ab plane. We used different scattering geometries (exploring the polarization dependences of magnetic intensities) and azimuthal scans around a magnetic reciprocal space point to determine without ambiguity that the moments are aligned approximately 18° away from the a axis. The temperature behaviors of the magnetic satellites have been probed at the $\left(0,\frac{1}{2},9\right)$ reciprocal node and show no evidence

of changes in the magnetic structure within the studied temperature range. Besides, an abrupt (non-power-law) decrease of magnetic intensities at T_N was found, consistent with the first order character of the antiferromagnetic transition of Sm$_2$IrIn$_8$. The resonance properties at the Sm L_2 and L_3 absorption edges revealed both resonant $E1$ and $E2$ process with roughly 1 order of magnitude more intense resonance peaks at the L_2 edge and a much stronger quadrupole resonance in the L_3 edge. The orientation of Sm moments in the ab plane and the small decrease of T_N compared to its value for SmIn$_3$ agree with a general CEF trend found in the $R_m M$In$_{3m+2}$ family.

*cadriano@ifi.unicamp.br

[1] H. Hegger, C. Petrovic, E. G. Moshopoulou, M. F. Hundley, J. L. Sarrao, Z. Fisk, and J. D. Thompson, Phys. Rev. Lett. **84**, 4986 (2000).

[2] C. Petrovic, R. Movshovich, M. Jaime, P. G. Pagliuso, M. F. Hundley, J. L. Sarrao, J. D. Thompson, and Z. Fisk, Europhys. Lett. **354-359**, 4986 (2001).

[3] C. Petrovic, P. G. Pagliuso, M. F. Hundley, R. Movshovich, J. L. Sarrao, J. D. Thompson, Z. Fisk, and P. Monthoux, J. Phys.: Condens. Matter **13**, L337 (2001).

[4] J. D. Thompson *et al.*, J. Magn. Magn. Mater. **226-230**, 5 (2001).

[5] P. G. Pagliuso, J. D. Thompson, M. F. Hundley, J. L. Sarrao, and Z. Fisk, Phys. Rev. B **63**, 054426 (2001).

[6] P. G. Pagliuso, J. D. Thompson, M. F. Hundley, and J. L. Sarrao, Phys. Rev. B **62**, 12266 (2000).

[7] R. Lora-Serrano, C. Giles, E. Granado, D. J. Garcia, E. Miranda, O. Agüero, L. Mendonça Ferreira, J. G. S. Duque, and P. G. Pagliuso, Phys. Rev. B **74**, 214404 (2006).

[8] G. Chen, S. Ohara, M. Hedo, Y. Uwatoko, K. Saito, M. Sorai, and I. Sakamoto, J. Phys. Soc. Jpn. **71**, 2836 (2002).

[9] E. G. Moshopoulou, Z. Fisk, J. L. Sarrao, and J. D. Thompson, J. Solid State Chem. **158**, 25 (2001).

[10] E. G. Moshopoulou, R. M. Ibberson, J. L. Sarrao, J. D. Thompson, and Z. Fisk, Acta Crystallogr., Sect. B: Struct. Sci. **62**, 173 (2006).

[11] K. H. J. Buschow, H. W. de Wijn, and A. M. van Diepen, J. Chem. Phys. **50**, 137 (1969).

[12] P. G. Pagliuso, C. Petrovic, R. Movshovich, D. Hall, M. F. Hundley, J. L. Sarrao, J. D. Thompson, and Z. Fisk, Phys. Rev. B **64**, 100503(R) (2001).

[13] P. G. Pagliuso, R. Movshovich, A. D. Bianchi, M. Nicklas, J. D. Thompson, M. F. Hundley, J. L. Sarrao, and Z. Fisk, Physica B **312-313**, 129 (2002).

[14] L. D. Pham, T. Park, S. Maquilon, J. D. Thompson, and Z. Fisk, Phys. Rev. Lett. **97**, 056404 (2006).

[15] V. S. Zapf, E. J. Freeman, E. D. Bauer, J. Petricka, C. Sirvent, N. A. Frederick, R. P. Dickey, and M. B. Maple, Phys. Rev. B **65**, 014506 (2001).

[16] T. Park, F. Ronning, H. Q. Yuan, M. B. Salamon, R. Movshovich, J. L. Sarrao, and J. D. Thompson, Nature (London) **440**, 65 (2006).

[17] V. A. Sidorov, M. Nicklas, P. G. Pagliuso, J. L. Sarrao, Y. Bang, A. V. Balatsky, and J. D. Thompson, Phys. Rev. Lett. **89**, 157004 (2002).

[18] A. Bianchi, R. Movshovich, I. Vekhter, P. G. Pagliuso, and J. L. Sarrao, Phys. Rev. Lett. **91**, 257001 (2003).

[19] E. D. Bauer, C. Capan, F. Ronning, R. Movshovich, J. D. Thompson, and J. L. Sarrao, Phys. Rev. Lett. **94**, 047001 (2005).

[20] J. Paglione, M. A. Tanatar, D. G. Hawthorn, E. Boaknin, R. W. Hill, F. Ronning, M. Sutherland, L. Taillefer, C. Petrovic, and P. C. Canfield, Phys. Rev. Lett. **91**, 246405 (2003).

[21] R. S. Kumar, A. L. Cornelius, and J. L. Sarrao, Phys. Rev. B **70**, 214526 (2004).

[22] N. Oeschler, P. Gegenwart, M. Lang, R. Movshovich, J. L. Sarrao, J. D. Thompson, and F. Steglich, Phys. Rev. Lett. **91**, 076402 (2003).

[23] A. D. Christianson *et al.*, Phys. Rev. B **70**, 134505 (2004).

[24] N. Harrison *et al.*, Phys. Rev. Lett. **93**, 186405 (2004).

[25] S. Raj *et al.*, Phys. Rev. B **71**, 224516 (2005).

[26] D. Hall, E. C. Palm, T. P. Murphy, S. W. Tozer, Z. Fisk, U. Alver, R. G. Goodrich, J. L. Sarrao, P. G. Pagliuso, and T. Ebihara, Phys. Rev. B **64**, 212508 (2001).

[27] D. Hall *et al.*, Phys. Rev. B **64**, 064506 (2001).

[28] J. Costa-Quintana and F. López-Aguilar, Phys. Rev. B **67**, 132507 (2003).

[29] J. L. Sarrao, L. A. Morales, J. D. Thompson, B. L. Scott, G. R. Stewart, F. Wastin, J. Rebizant, P. Boulet, E. Colineau, and G. H. Lander, Nature (London) **420**, 297 (2002).

[30] E. D. Bauer *et al.*, Phys. Rev. Lett. **93**, 147005 (2004).

[31] A. D. Christianson *et al.*, Phys. Rev. Lett. **95**, 217002 (2005).

[32] R. Lora-Serrano, L. Mendonça Ferreira, D. J. Garcia, E. Miranda, C. Giles, J. G. S. Duque, E. Granado, and P. G. Pagliuso, Physica B **384**, 326 (2006).

[33] N. V. Hieu *et al.*, J. Phys. Soc. Jpn. **75**, 074708 (2006).

[34] A. Malinowski, M. F. Hundley, N. O. Moreno, P. G. Pagliuso, J. L. Sarrao, and J. D. Thompson, Phys. Rev. B **68**, 184419 (2003).

[35] V. F. Correa, L. Tung, S. M. Hollen, P. G. Pagliuso, N. O. Moreno, J. C. Lashley, J. L. Sarrao, and A. H. Lacerda, Phys. Rev. B **69**, 174424 (2004).

[36] E. Granado, P. G. Pagliuso, C. Giles, R. Lora-Serrano, F. Yokaichiya, and J. L. Sarrao, Phys. Rev. B **69**, 144411 (2004).

[37] P. G. Pagliuso *et al.*, J. Appl. Phys. **99**, 08P703 (2006).

[38] W. Bao, P. G. Pagliuso, J. L. Sarrao, J. D. Thompson, Z. Fisk, J.

W. Lynn, and R. W. Erwin, Phys. Rev. B **62**, R14621 (2000); **63**, 219901(E) (2001).

[39] W. Bao, P. G. Pagliuso, J. L. Sarrao, J. D. Thompson, Z. Fisk, and J. W. Lynn, Phys. Rev. B **64**, 020401(R) (2001).

[40] S. Chang, P. G. Pagliuso, W. Bao, J. S. Gardner, I. P. Swainson, J. L. Sarrao, and H. Nakotte, Phys. Rev. B **66**, 132417 (2002).

[41] E. Granado, B. Uchoa, A. Malachias, R. Lora-Serrano, P. G. Pagliuso, and H. Westfahl, Jr., Phys. Rev. B **74**, 214428 (2006).

[42] M. Kasaya, B. Liu, M. Sera, T. Kasuya, D. Endoh, T. Goto, and F. Fujimura, J. Magn. Magn. Mater. **52**, 289 (1985).

[43] D. Endoh, T. Goto, A. Tamaki, B. Liu, M. Kasaya, T. Fujimura, and T. Kasuya, J. Phys. Soc. Jpn. **58**, 940 (1989).

[44] Z. Kletowski, J. Magn. Magn. Mater. **186**, L7 (1998).

[45] A. Stunault, K. Dumesnil, C. Dufour, C. Vettier, and N. Bernhoeft, Phys. Rev. B **65**, 064436 (2002).

[46] Z. Fisk and J. P. Remeika, in *Handbook on the Physics and Chemistry of Rare Earths*, edited by J. K. A. Geschneider and E.

L. Eyring (Elsevier, Amsterdam/North-Holland, Amsterdam, 1989), Vol. 12, p. 53.

[47] L. Paolasini *et al.*, J. Synchrotron Radiat. **14**, 301 (2007).

[48] J. P. Hill and D. F. McMorrow, Acta Crystallogr., Sect. A: Found. Crystallogr. **A52**, 236 (1996).

[49] A. Zheludev, J. P. Hill, and D. J. Buttrey, Phys. Rev. B **54**, 7216 (1996).

[50] J. P. Hill, A. Vigliante, D. Gibbs, J. L. Peng, and R. L. Greene, Phys. Rev. B **52**, 6575 (1995).

[51] C. Detlefs, A. H. M. Z. Islam, A. I. Goldman, C. Stassis, P. C. Canfield, J. P. Hill, and D. Gibbs, Phys. Rev. B **55**, R680 (1997).

[52] J. P. Hannon, G. T. Trammell, M. Blume, and D. Gibbs, Phys. Rev. Lett. **61**, 1245 (1988).

[53] M. Blume and D. Gibbs, Phys. Rev. B **37**, 1779 (1988).

[54] K. Kubo and T. Hotta, J. Phys. Soc. Jpn. **75**, 083702 (2006).

[55] T. Tsuchida and W. E. Wallace, J. Chem. Phys. **43**, 3811 (1965).